


RESEARCH ARTICLE

Ex-vivo fluorescence confocal microscopy with digital staining for characterizing basal cell carcinoma on frozen sections: A comparison with histology

Cristel Ruini^{1,2*}  | Gabriela Vladimirova¹ | Benjamin Kendziora¹ |
Suzanna Salzer¹ | Ecem Ergun¹ | Elke Sattler¹ | Lars E. French^{1,3} |
Daniela Hartmann¹

¹Department of Dermatology and Allergy, University Hospital, LMU Munich, Germany

²PhD School in Clinical and Experimental Medicine, University of Modena and Reggio Emilia, Italy

³Dr. Phillip Frost Department of Dermatology & Cutaneous Surgery, University of Miami, Miller School of Medicine, Miami, Florida

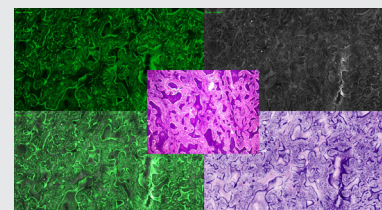
*Correspondence

Cristel Ruini, Department of Dermatology and Allergy, University Hospital, LMU Munich, Frauenlobstr 9-11, 80337 Munich, Germany.

Email: cristel.ruini@med.uni-muenchen.de

Abstract

Ex-vivo fluorescence confocal microscopy (FCM) has been used on fresh tissue, but there is little experience on frozen sections. We evaluated the applicability of FCM on frozen sections of basal cell carcinomas (BCCs), stained with acridine orange and digitally colored to simulate hematoxylin and eosin (H&E) dyes. We compared our diagnostic accuracy in detecting and subtyping BCCs with FCM to our gold standard (H&E stained frozen sections used in 3D horizontal micrographic surgery). Forty-six primary BCCs were analyzed for free margins as well as histological subtype with all FCM modes and conventional H&E staining. Adnexa, artifacts and diagnostic confidence were evaluated. Free margins were identified with a sensitivity and specificity of 92% and 91%. Concordance for tumor subtype was 88%. FCM may be used on both fresh tissue and frozen samples, although with reduced performance and different artifacts. The device is useful for the intraoperative diagnosis, subtyping and margin-mapping of BCCs.



KEYWORDS

basal cell carcinoma, bedside histology, digital staining, ex-vivo confocal microscopy, micrographic surgery

Abbreviations: BCC, Basal cell carcinoma; DS, digital staining; FCM, ex-vivo fluorescence confocal microscopy; FM, fluorescence mode; hematoxylin & eosin, (H&E); MMS, Mohs micrographic surgery; OM, overlap mode; RM, reflectance mode.

This is an open access article under the terms of the Creative Commons Attribution License, which permits use, distribution and reproduction in any medium, provided the original work is properly cited.

© 2021 The Authors. *Journal of Biophotonics* published by Wiley-VCH GmbH.

1 | INTRODUCTION

Basal cell carcinoma (BCC) accounts for about 80% of epithelial skin tumors. One of the most effective treatments of BCC is Mohs micrographic surgery (MMS) with analysis of frozen sections, which is associated with lower recurrence rates. MMS, derived from the original Mohs

chemosurgery developed by the general surgeon Frederic E. Mohs in 1938 [1], is carried out with different variations (whole piece or PacMan, Munich method, Margin strip method, Muffin technique) [2, 3], but always in multiple steps. It requires trained dermatosurgeons and technicians, as well as specialized laboratory facilities. The Munich method is performed sequentially on multiple days; the cylindrical excised tissue is cut into horizontal sections with a cryostat and successively stained with hematoxylin & eosin (H&E). Numerous sections must be assessed and the visualization of the epidermis might be limited; however, complete excision can be confirmed by visualization of the entire tumor (3D) [2, 3].

Ex-vivo fluorescence confocal microscopy (FCM) was successfully used for margin mapping of BCCs and other tumors, such as melanoma, squamous cell carcinoma [4–7], prostate and breast cancer [8–11]. It was also employed for the characterization of autoimmune and inflammatory skin diseases such as pemphigus, pemphigoid, lichen planus, lupus erythematosus and vasculitis [12–18].

FCM consists of a confocal microscope with two lasers of different wavelengths, providing images in reflectance (RM) and fluorescence mode (FM). The latest generation device is also equipped with an overlap between the two modes (OM) and a digital staining (DS) software.

Due to its high sensitivity (up to 88%) and specificity (up to 99%) for the diagnosis of BCC on fresh tissue stained with acridine orange [19], FCM is now a recognized, appealing alternative to conventional frozen histology used in Mohs surgery. There are, however, no studies on the applicability of this technique to frozen sections instead of fresh tissue and in the context of variants of micrographic surgery such as the Munich method.

In this study, we therefore evaluated the applicability of FCM on frozen sections of BCCs, stained with acridine orange and digitally colored to simulate H&E dyes, describing more common artifacts encountered in the process. Moreover, we sought to prospectively assess in a clinical setting, our sensitivity and specificity in detecting and subtyping BCCs using FCM compared to our gold standard (H&E stained frozen sections used in 3D horizontal micrographic surgery).

2 | MATERIALS AND METHODS

2.1 | Population, samples and devices

Forty-six consecutive patients with histologically diagnosed BCC and planned for micrographic surgery in the Munich method variant were enrolled in the study between November 2018 and June 2019. A 35 μm thick horizontal frozen sections of primary BCCs were

collected immediately after tissue processing and subsequently stained. The staining process included a complete and homogeneous tissue incubation in: 10% citric acid, Dulbecco's Phosphate buffered saline (both Sigma-Aldrich), acridine orange (0.6 mM; Sigma-Aldrich) and again Dulbecco's Phosphate buffered saline. Each step lasted 30 seconds. After staining, 1024×1024 pixels images (single field of view: $550 \mu\text{m}^2$, maximum mosaic area: 25mm^2) were acquired with FCM Vivascope 2500[®]4G (Mavig GmbH, Munich, Germany). Acquisition time was 1 to 2 minutes. Images were analyzed in RM, FM, OM and with DS by two independent, blinded dermatologists with experience in dermatosurgery, imaging and dermatopathology. Concordance rate was high (87%). In discordant cases, a third senior dermatosurgeon, expert in imaging and trained in dermatopathology was involved.

Following FCM acquisition, frozen sections were H&E stained and blinded evaluated by two dermatologists experienced in dermatohistopathology (concordance 95.6%; in case of discordance, the final decision was taken by the senior examiner).

The following parameters were evaluated in all FCM modi and in H&E staining: Complete or partial resection, histological subtype, presence of scars, adnexal structures (sweat glands, sebaceous glands, hair follicles), fat tissue, muscle, artifacts.

The grades of confidence of the examiner were also evaluated (1 = high, >75%, 2 = average, 75%-50% confidence, 3 = low, <50% confidence, 4 = indeterminate).

The study followed the Declaration of Helsinki and pre-operative written informed consent was acquired from each patient. All pseudonymised images were stored on a study-dedicated hard drive. The project was approved by the Ethics Committee of the Ludwig Maximilian University (LMU), Munich, Germany (Nr. 19-150).

2.2 | Statistical analysis

For descriptive statistics, mean values with SD were calculated for numeric variables, while absolute numbers with percentage values were listed for nominal variables. To evaluate the diagnostic accuracy of FCM in detecting different BCC subtypes and histological characteristics, the sensitivity, specificity, positive predictive value, negative predictive value, and area under the curve (AUC) of the receiver operating characteristic (ROC) curve were calculated. Pearson's chi-squared test was used to evaluate a possible correlation between artifacts in FCM and limited quality in dermatohistopathology. The effects of FCM mode qualities on in toto and subtype agreement were evaluated using logistic regression models. *P*-values <.05 were considered statistically significant. R (version

TABLE 1 Patients' cohort

Age, mean years (SD)	74.4 (11.1)
Female, % (n)	39.1 (18/46)
Male, % (n)	60.9 (28/46)
Location	
Forehead % (n)	21.7 (10/46)
Cheek % (n)	21.7 (10/46)
Dorsum nasi % (n)	4.3 (2/46)
Ala nasi % (n)	15.2 (7/46)
Ear % (n)	6.5 (3/46)
Retroauricular/neck, % (n)	6.5 (3/46)
Scalp % (n)	13.0 (6/46)
Upper lip, % (n)	6.5 (3/46)
Chin % (n)	4.3 (2/46)

3.6.0, 2019, R Foundation for Statistical Computing) was used for all statistical calculations.

3 | RESULTS AND DISCUSSION

3.1 | Results

3.1.1 | Population

Forty-six patients (18 females and 28 males with a mean age of 74 ± 11 years) with BCC of the head and neck region were enrolled (Table 1). The included BCC subtypes were: Nodular and micronodular (23), superficial (1), infiltrating (8), mixed type nodular infiltrating (9), mixed type nodular baso-squamous (1). (Table 2).

3.1.2 | BCCs diagnostic agreement

Using FCM, we could determine whether the tumor was completely excised with a sensitivity of 92% (95% CI: 73-99), and a specificity of 91% (71-99); Kappa: 0.83 (0.66-0.99), AUC: 0.91(83-100), when compared to conventional H&E staining (Table 3). If only non-radical excisions are taken into account however, we could perfectly identify the exact margins only in 66% (42-83) of the cases, otherwise undergoing under- (5/10) or over-estimation (5/10).

3.1.3 | BCC subtype agreement

The overall agreement between frozen sections and FCM in determining the BCC subtype was 88% (95% CI: 74-

TABLE 2 BCC Subtypes

Subtype	H&E	FCM
Nodular, % (n)	50 (23/46)	58.7 (27/46)
Morpheaform % (n)	17.4 (8/46)	15.2 (7/46)
Superficial multicentric % (n)	2.2 (1/46)	2.2 (1/46)
Nodular + morpheaform % (n)	19.6 (9/46)	10.9 (5/46)
Nodular basosquamous % (n)	2.2 (1/46)	2.2 (1/46)
No tumor % (n)	8.7 (4/46)	8.7 (4/46)
Not evaluable % (n)	0 (0/46)	2.2 (1/46)

Abbreviation: BCC, basal cell carcinoma.

96). The sensitivity of FCM in detecting nodular subtypes was 100% (86-100), with a specificity of 82% (60-95); Kappa: 0.82 (0.66-0.99), AUC: 0.91(0.83-1.00). The sensitivity of FCM in detecting infiltrating subtypes was 88% (47-100), with a specificity of 100% (91-100); Kappa: 0.92 (0.77-0.92), AUC: 0.94 (0.82-1.00). The sensitivity of FCM in detecting mixed subtypes was 56% (21-86), with a specificity of 100% (91-100); Kappa: 0.67 (0.37-0.96), AUC: 0.78 (0.61-0.95). (Table 3).

3.1.4 | Additional histopathological features

The sensibility and specificity for the typical BCC key features were: 94% (95% CI: 81-99) and 78% (95% CI: 40-97) for stromal reaction, 97% (95% CI: 82-100) and 73% (95% CI: 45-92) for palisading and 97% (95% CI: 82-100) and 87% (95% CI: 60-98) for clefting.

Moreover, with FCM we were able to correctly identify further anatomical structures with high sensitivity and specificity: scars (88%; 95%), fat tissue (92%; 71%). The sensitivity for adnexa was 98%, the specificity was not calculable since every sample actually contained adnexal structures. Muscle and cartilage could also be correctly identified by means of FCM, their sample size was, however, too low for statistical analysis (Table 2) (Figure 5).

3.1.5 | Artifacts and quality

Most slides were reported as good (54%), or average (41%), with just 4% judged as poor. All histopathological slides could be evaluated. In the FCM images, one or more artifacts were present in 61% of cases, with slight blurring in 33%, ill-defined borders in 30%, cutting artifacts in 28% and square blocks (altered mosaic reconstruction) visible in 13% of the cases. A chi-square test showed no significant association between limited quality

TABLE 3 Diagnostic accuracy with FCM

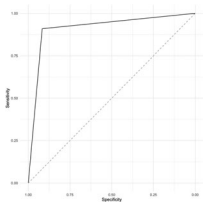
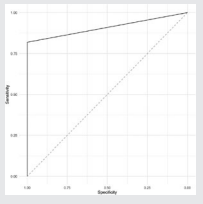
Point estimates and 95% CIs: in detecting a complete BCC resection	
Apparent prevalence	0.52 (0.37, 0.67)
True prevalence	0.52 (0.37, 0.67)
Sensitivity	0.92 (0.73, 0.99)
Specificity	0.91 (0.71, 0.99)
Positive predictive value	0.92 (0.73, 0.99)
Negative predictive value	0.91 (0.71, 0.99)
Positive likelihood ratio	10.08 (2.68, 38.01)
Negative likelihood ratio	0.09 (0.02, 0.35)
Kappa	0.83 (95% CI: 0.66, 0.99)
AUC	0.91(95% CI: 0.83, 1.00)
ROC Curve	in detecting nodular BCC subtypes
	
Apparent prevalence	0.61 (0.45, 0.75)
True prevalence	0.52 (0.37, 0.67)
Sensitivity	1.00 (0.86, 1.00)
Specificity	0.82 (0.60, 0.95)
Positive predictive value	0.86 (0.67, 0.96)
Negative predictive value	1.00 (0.81, 1.00)
Positive likelihood ratio	5.50 (2.27, 13.35)
Negative likelihood ratio	0.00 (0.00, NaN)
Kappa	0.82 (95% CI: 0.66, 0.99)
AUC	0.91(95% CI: 0.83, 1.00)
ROC Curve	in detecting mixed BCC subtypes
	
Apparent prevalence	0.11 (0.04, 0.24)
True prevalence	0.20 (0.09, 0.34)
Sensitivity	0.56 (0.21, 0.86)
Specificity	1.00 (0.91, 1.00)
Positive predictive value	1.00 (0.48, 1.00)
Negative predictive value	0.90 (0.77, 0.97)
Positive likelihood ratio	Inf (NaN, Inf)
Negative likelihood ratio	0.44 (0.21, 0.92)
Kappa	0.67 (95% CI: 0.37, 0.96)
AUC	0.78 (95% CI: 0.61, 0.95)

TABLE 3 (Continued)

Point estimates and 95% CIs: in detecting a complete BCC resection	
ROC Curve	in detecting infiltrative subtypes
Apparent prevalence	0.15 (0.06, 0.29)
True prevalence	0.17 (0.08, 0.31)
Sensitivity	0.88 (0.47, 1.00)
Specificity	1.00 (0.91, 1.00)
Positive predictive value	1.00 (0.59, 1.00)
Negative predictive value	0.97 (0.87, 1.00)
Positive likelihood ratio	Inf (NaN, Inf)
Negative likelihood ratio	0.12 (0.02, 0.78)
Kappa	0.92 (95% CI: 0.77, 0.92)
AUC	0.94 (95% CI: 0.82, 1.00)
ROC Curve	

Abbreviation: AUC, area under the curve; BCC, basal cell carcinoma; CI, 95% confidence interval; FCM, ex-vivo confocal laser scanning microscopy; Inf, infinity; NaN, not a number; ROC, receiver operating characteristic.

in conventional histopathology and one or more artifacts in FCM, $X^2(1, N = 46) = 0.29, P = .590$.

3.1.6 | Diagnostic confidence

The diagnostic confidence of the FCM images based on the quality of the acquired images was good-average in 91% FM, 93.5% RM and OM, and in 93% of DS images. Poor confidence was reported in 4% FM, 6% RM and OM and 2% DS images. Moreover, in 2 cases (4%) DS and FM were not evaluated due to lack of staining. In 93%, the observers found DS useful in confirming their diagnose.

Logistic regression models did not show a significant effect of the FM quality ($P = .596, P = .995$), RM quality ($P = .995, P = .998$), OM quality ($P = .995, P = .998$), or DS mode quality ($P = .301, P = .996$) on in toto agreement or on BCC subtype agreement.

3.2 | DISCUSSION

FCM is considered a promising tool for quick and cost-effective bedside surgery, enabling reoperations and/or wound closures within a substantially shorter time frame and in an “one-step procedure” compared to standard frozen sections. The latest generation FCM device uses two laser wavelengths of 488 nm (blue) and 758 nm (infrared). The blue laser excites fluorescent dyes, such as acridine orange, and marks nuclear structures, which appear green in FM. Meanwhile, the infrared laser generates a reflectance signal that highlights chromophores such as melanin and keratin, which appear in different shades of gray in RM. FCM images can be interpreted only after a dedicated training, even by Mohs surgeons and dermatopathologists. Numerous artifacts can further complicate the correct FCM assessment [4, 20–23]. For this reason, room for improvement remains.

The introduction of the new digital staining software in the fourth generation of FCM represents a breakthrough, since it produces a multimodal pseudo-color image mimicking H&E. The dedicated DS software color maps cell nuclei in blue and the extracellular matrix and cytoplasm in pink. As a consequence, the user can experience a direct and intuitive comparison to the standard H&E features. A pilot study on healthy skin reported a very high correlation between digitally stained FCM mosaics and H&E sections, although no statistical analysis was provided [24]. The authors could correlate the morphology of main skin structures, including appendages, and even noticed a better visualization of adipocytes and hair follicles. (Figure 5).

Our study was the first to include the digital staining feature in assessing a large series of BCCs and to apply FCM on frozen tissue slides, excised with the Munich method. Although FCM has been conceived for the use on fresh tissue in fact, the applicability on frozen sections could be useful in case a quick re-evaluation of already stored but not yet H&E stained specimens is needed. Moreover, the whole frozen tissue block can be rapidly analyzed with FCM, since staining with acridine orange is quicker than paraffin inclusion and H&E processing. After the preliminary FCM screening, selected tissue

slides might be H&E or immunostained and further examined.

Using FCM, we were able to correctly identify free resection margins with high sensitivity and specificity (92%;91%), compared to H&E stained frozen sections used in our gold standard 3D-horizontal micrographic surgery. These results are in line with previously published studies on fresh tissue [19, 25, 26].

We were also able to determine the subtype of the excised BCCs (Figure 1-4). Nodular BCCs were clearly visible as ovoid tumor nests, colored in blue in DS (Figure 1), while strands and cords surrounded by a rich stroma were present in infiltrating BCCs (Figure 2). FCM was more sensitive in recognizing nodular subtypes, but more specific with regard to infiltrative subtypes. Mixed subtypes were more difficult to diagnose than pure subtypes (sensitivity 56%, specificity 100%). The only case of superficial BCC and baso-squamous carcinoma could be correctly identified.

In accordance with the first study on DS of healthy skin [24], we could visualize the main anatomical structures, as in H&E slides, with high concordance rates. Fat tissue was visible in every mode as an aggregation of empty, lobulated spaces with bright (blue-lilac in DS) nuclear elements pushed to the periphery; muscle fibers

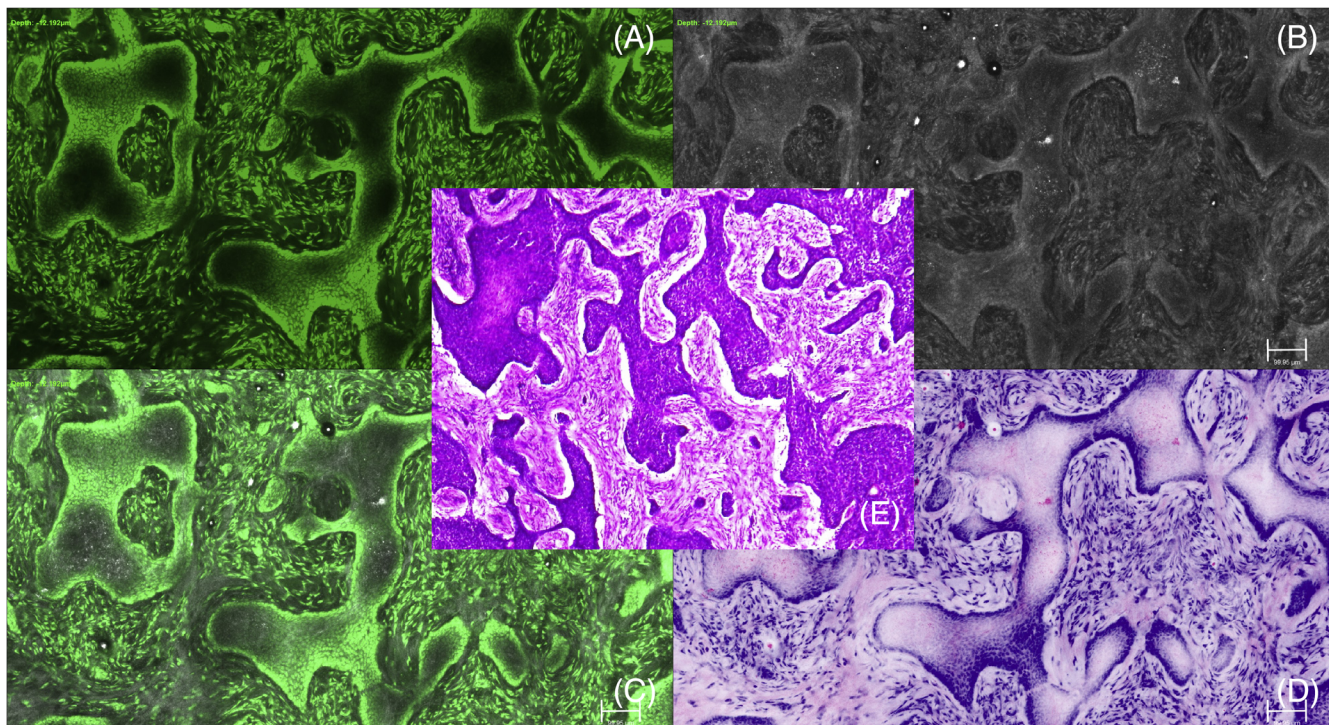


FIGURE 1 Infiltrative BCC in FCM FM (A), RM (B), OM (C), DS (D) and H&E 10x (E). Note the typical infiltrative cords, colored in blue-lilac in DS (D) and H&E (E), with palisading of the peripheral nuclei, surrounded by empty spaces (clefting), and stromal reaction. BCC, basal cell carcinoma; DS, digital staining; H&E, hematoxylin and eosin; FCM, ex-vivo confocal laser scanning microscopy; FM, fluorescence mode; OM, overlap mode; RM, reflectance mode

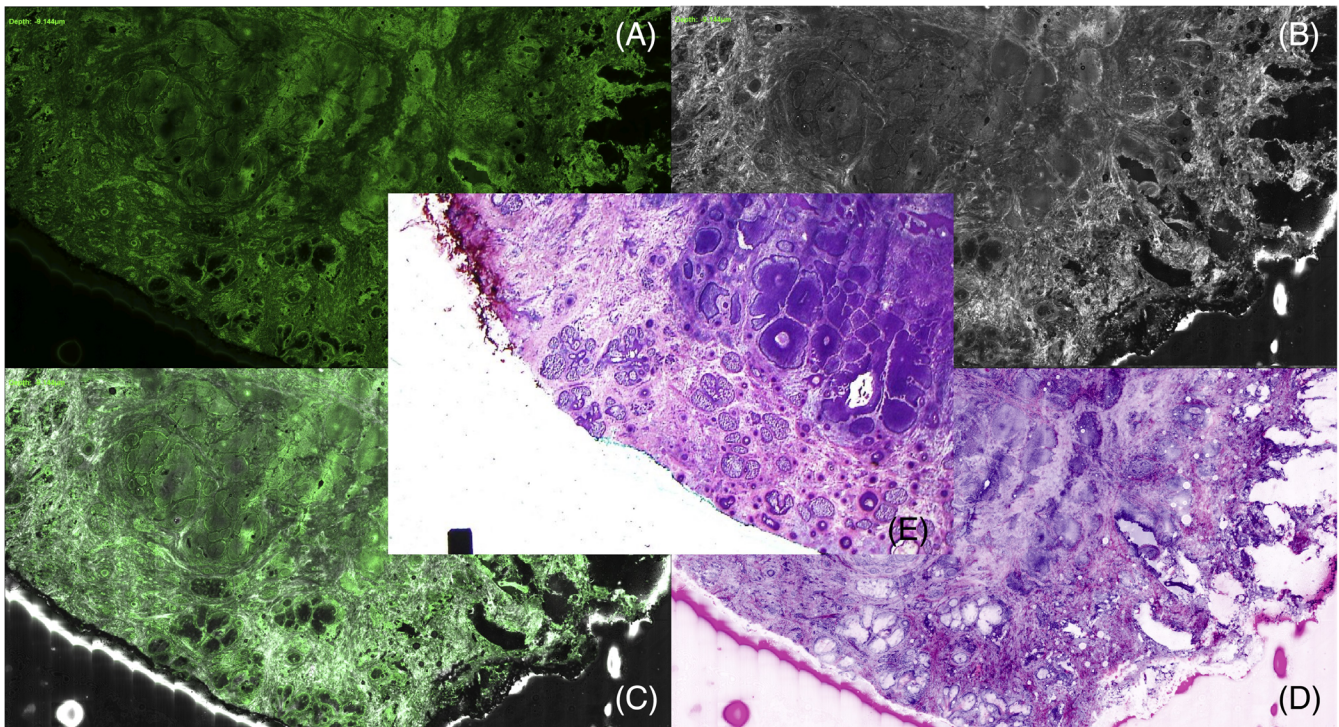


FIGURE 2 Nodular BCC in FCM FM (A), RM (B), OM (C), DS (D) and H&E $\times 1.25$ (E), completely excised. Note the typical nodular tumor islands, colored in blue-lilac in DS (D) and H&E (E), surrounded by empty spaces (clefting) and stromal reaction. Sebaceous glands are also visible as acinar structures. BCC, basal cell carcinoma; DS, digital staining; H&E, hematoxylin and eosin; FCM, ex-vivo confocal laser scanning microscopy; FM, fluorescence mode; OM, overlap mode; RM, reflectance mode

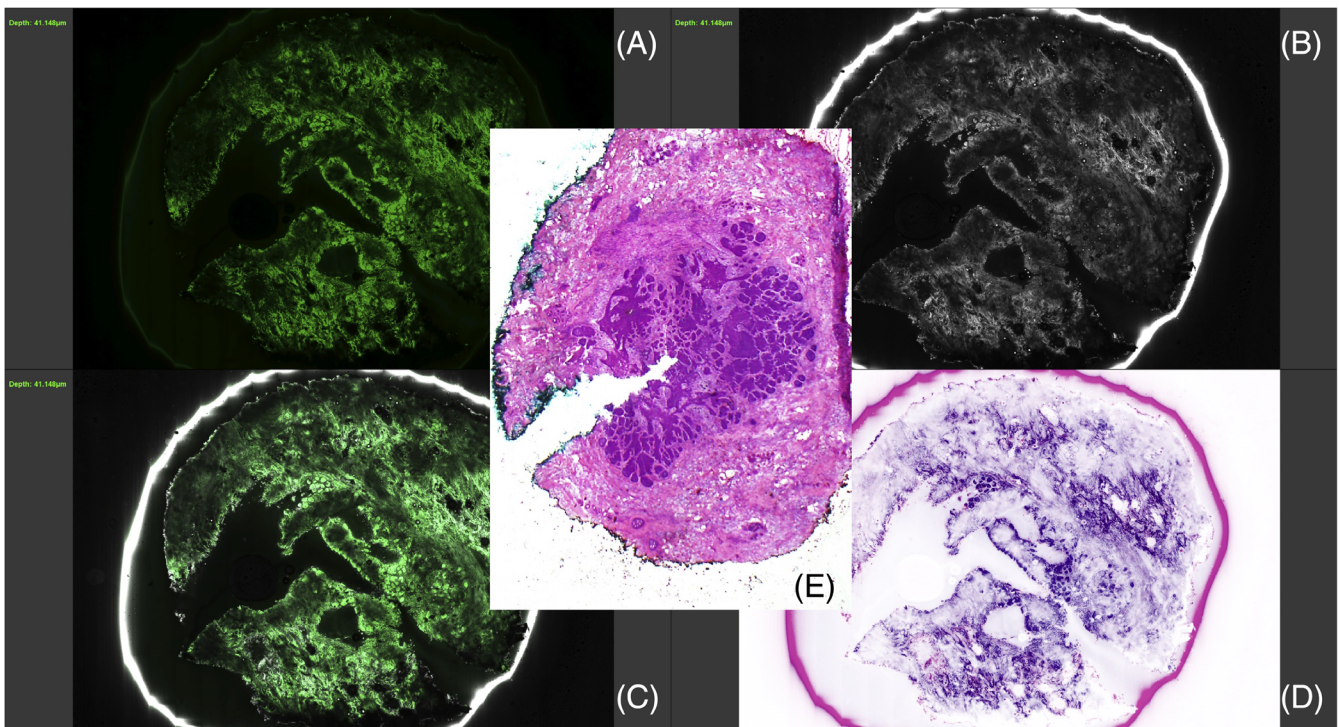


FIGURE 3 Micronodular BCC in FCM FM (A), RM (B), OM (C), DS (D) and H&E $\times 1.25$ (E), completely excised. Note the tumor micronodules colored in blue-lilac in DS (D) and H&E (E), surrounded by empty spaces (clefting) and stromal reaction. Sebaceous and sweat glands are also visible. Note the cut indicating the slide orientation at 12 o'clock. BCC, basal cell carcinoma; DS, digital staining; H&E, hematoxylin and eosin; FCM, ex-vivo confocal laser scanning microscopy; FM, fluorescence mode; OM, overlap mode; RM, reflectance mode

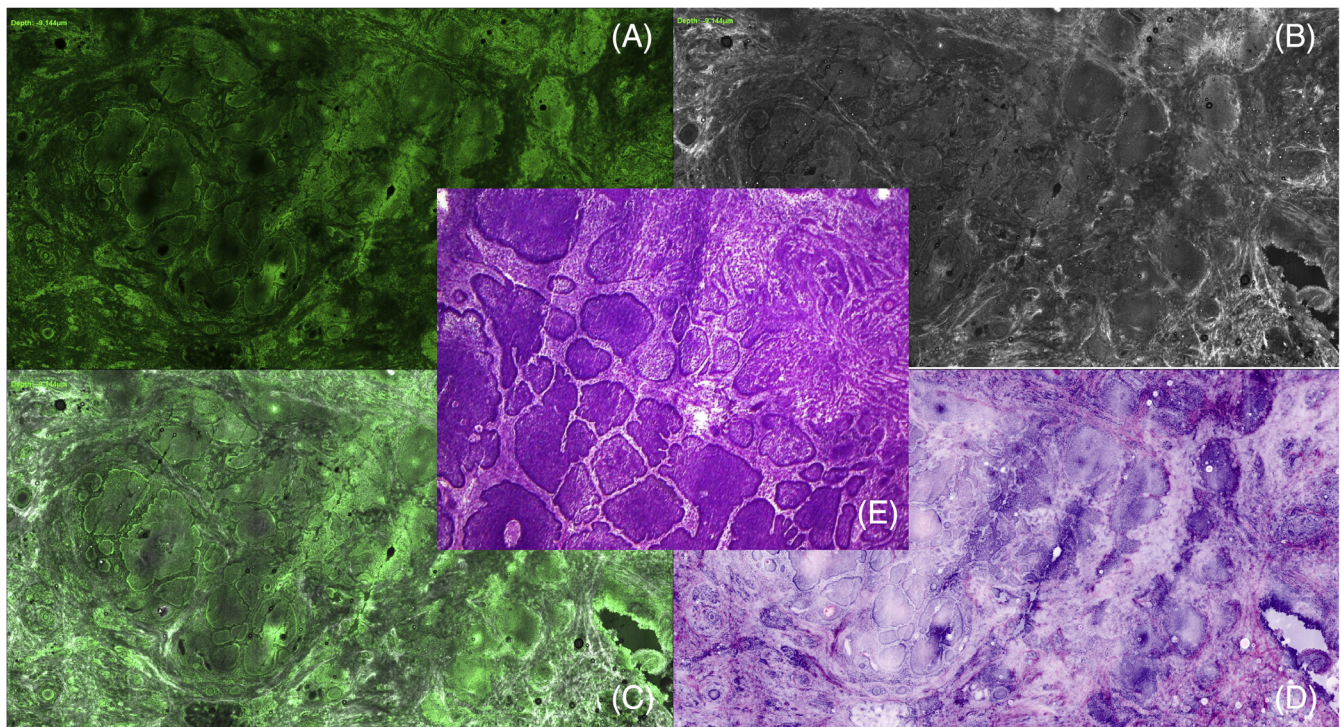


FIGURE 4 Nodular-micronodular BCC in FCM FM (A), RM (B), OM (C), DS (D) and H&E $\times 4$ (E), completely excised. Note the typical nodular tumor islands, colored in blue-lilac in DS (D) and H&E (E), surrounded by empty spaces (clefting) and stromal reaction. Sebaceous glands are also visible as acinar structures. BCC, basal cell carcinoma; DS, digital staining; H&E, hematoxylin and eosin; FCM, ex-vivo confocal laser scanning microscopy; FM, fluorescence mode; OM, overlap mode; RM, reflectance mode

were displayed as elongated elements with bright (blue-lilac in DS) nucleus, while connective tissue in scars had a pink appearance in DS. Adnexae (including hair follicles, sebaceous glands, eccrine sweat glands) were correctly identified, colored blue-lilac in DS. (Figure 5).

Compared to fresh tissue, we noticed a high prevalence of artifacts (61% of FCM examined samples). At this regard, it is important to underline the differences between the types of artifacts that should be expected using frozen sections compared to fresh tissue. In conventional FCM on fresh tissue in fact, artifacts usually arise from either staining anomalies or irregular tissue plane embedding and flattening, which can curl the epidermis. This brings to halos/blurring, black holes and imperfect mosaic stitching in the image [23]. On the other side, artifacts in frozen sections seem to mainly arise from irregular distribution of fluorescent dye and from the microtome knife. We mainly noticed blurring and ill-defined borders due to fuzzy staining, probably because of an inhomogeneous distribution of acridine orange in the frozen sections. On the other hand, microtome cutting artifacts, corresponding to tears or cracks in the tissue (as if tissue elements had separate and fractured) were seen in both FCM images and H&E slides, and should be attributed to cryosectioning and overstretching of the tissue [27].

Interestingly, artifacts did not seem to significantly limit the overall examination and did not correlate with lower diagnostic confidence. Besides artifacts, additional issues might compromise a correct evaluation of FCM images; in particular, the loss of small tumor foci during stitching of single images into mosaics (due to imperfect alignment) and the, sometimes tricky, differential diagnosis between BCC and sebaceous glands [21, 23, 28].

Our diagnostic confidence was good-average in $>90\%$ cases. Compared with the earlier generation of FCM, just offering FM and RM, we experienced a more accurate evaluation of the images owing to OM and DS. In fact, OM combines the two FM/RM modes into one image, providing an enhancement of both cytoplasmic and nuclear structures, thereby improving the overall visualization of the sample, especially at the margins. On the other hand, DS immediately reminds the user of classical H&E stained slides, and makes the evaluation more intuitive. In 93.5% of cases, the authors found DS useful for diagnosing not only BCCs, but also additional anatomical structures such as glands.

Time efficiency is a noteworthy aspect in FCM. MMS processing requires, depending on the technique used, 20 minutes to 1 hour. The staining time with H&E varies

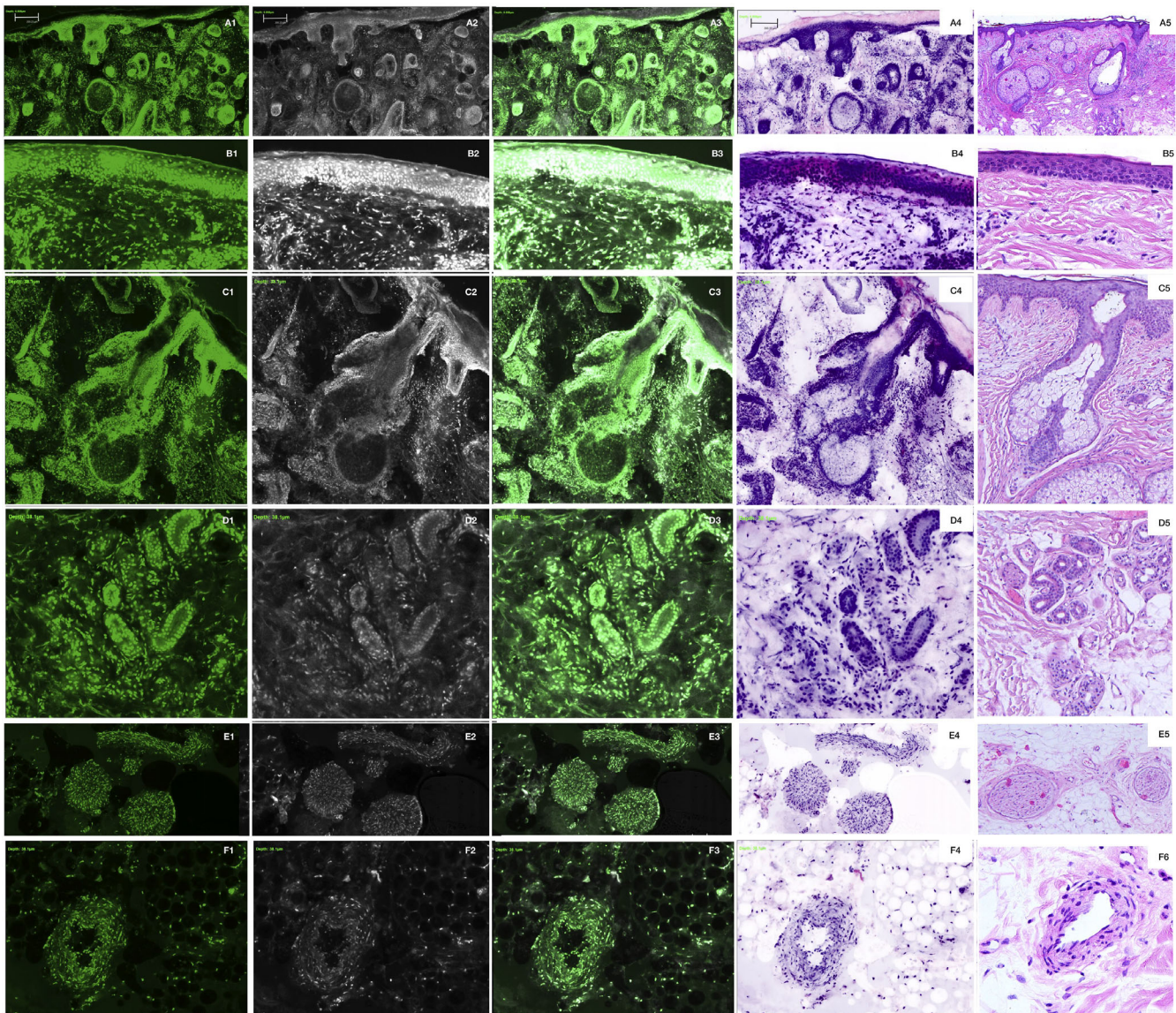


FIGURE 5 Healthy skin (A) showing the epidermal layer and the underlying dermis with hair follicles; Epidermis with multiple layers of keratinocytes (B); hair follicle with its sebaceous gland (C); sweat gland with its typical double layering of cells (D); section of a nerve (E); arteriole with its lumen and tunica intima, media and adventitia (F), surrounded by fat tissue with multiple adipocyte with their peripheral nuclei in FCM FM (1), RM (2), OM (3), DS (4) and H&E $\times 4$ (5). BCC, basal cell carcinoma; DS, digital staining; H&E, hematoxylin and eosin; FCM, ex-vivo confocal laser scanning microscopy; FM, fluorescence mode; OM, overlap mode; RM, reflectance mode

between 5 and 7 minutes. Since FCM can be used on fresh tissue, the time needed for the standard staining protocols with acetic acid, buffered saline solution and acridine orange is reduced to 20 seconds for each step. Depending on the sample size, complete image acquisition requires between 1 and 3 minutes. Since there is no damage to the tissue, samples may also be sent for conventional histopathology for further examination, if needed.

This study has some limitations; first of all, the small sample size due to its pilot nature; moreover, the anatomical location of the analyzed tumors, all arising in the head and neck area. This corresponds however to the real life context of micrographic surgery in our

hospital, since BCCs of other sites are usually excised with conventional surgery.

4 | CONCLUSION

We aimed to verify whether not only fresh tissue, but also frozen sections could be stained with acridine orange and efficiently analyzed with FCM with DS. We observed a higher frequency of artifacts due to inhomogeneous staining and microtome cutting. We still achieved a very high sensitivity (92%) and specificity (91%) for detecting free margins and determining BCC

subtypes (88%), but we were less accurate (65%) in the exact identification of margins in case of incomplete resection. Although we believe FCM should be used on fresh tissue to ensure its maximal potential, the use on frozen sections could be useful in specific settings such as retrospective reviews and second opinions.

Nevertheless, we highlighted the value of the new generation FCM in the context of micrographic surgery of BCC. Using FCM with OM and DS, it is possible to visualize BCCs and surrounding anatomical structures with high sensitivity and specificity, determine the tumor subtype and the extent of excision in the context of micrographic surgery with the Munich method variant. The novel DS tool simulates H&E stained histological sections and provides additional information for the overall assessment of BCCs.

Larger studies are needed to further investigate the potential of FCM, to improve the staining and DS algorithms, reduce the artifacts and to systematically assess the time- and cost-efficiency of this technique.

ACKNOWLEDGMENTS

The authors thank Mavig GmbH (Munich, Germany) for providing the Vivascope 2500 device for this study. Open Access funding enabled and organized by ProjektDEAL.

CONFLICT OF INTERESTS

Daniela Hartmann and Cristel Ruini occasionally received honoraria from Mavig GmbH for international training courses on confocal microscopy. All authors declare to have no relevant conflict of interest.

AUTHOR CONTRIBUTIONS

Cristel Ruini (writing, recruitment, data analysis), Gabriela Vladimirova (data collection), Benjamin Kendziora (statistical analysis), Ecem Ergun (data collection), Suzanna Salzer (editing), Lars E. French (editing), Elke Sattler (editing), Daniela Hartmann (recruitment, data analysis, idea, editing, senior coordination).

DATA AVAILABILITY STATEMENT

Fully anonymised data that support the findings of this study are available from the corresponding author upon reasonable request.

ORCID

Cristel Ruini  <https://orcid.org/0000-0002-9860-1095>

REFERENCES

- [1] F. E. Mohs, *Arch. Surg.* **1941**, *42*, 279.
- [2] J. Paoli, O. Cogrel, S. V. D. Geer, G. Krekels, J. D. Leeuw, Matthias, Moehrle, J. U. Ostertag, L. R. Buceta, N. Sheth, S. Lächli in ESMS position document on the use of mohs micrographic surgery and other micrographic surgery techniques in Europe, **2019**.
- [3] L. F. Kopke, B. Konz, *Hautarzt* **1995**, *46*, 607.
- [4] J. Perez-Anker, J. Malvey, D. Moreno-Ramirez, *Actas Dermosifiliogr* **2020**, *111*, 236.
- [5] D. Hartmann, S. Krammer, M. R. Bachmann, L. Mathemeier, T. Ruzicka, I. S. Bagci, T. von Braunmuhl, *J. Biophotonics* **2018**, *11*, e201700318.
- [6] D. Hartmann, S. Krammer, S. Vural, M. R. Bachmann, C. Ruini, M. Sardy, T. Ruzicka, C. Berking, T. von Braunmuhl, *J. Biophotonics* **2018**, *11*.
- [7] D. Hartmann, C. Ruini, L. Mathemeier, M. R. Bachmann, A. Dietrich, T. Ruzicka, T. von Braunmuhl, *J. Biophotonics* **2017**, *10*, 128.
- [8] L. Bertoni, S. Puliatti, L. Reggiani Bonetti, A. Maiorana, A. Eissa, P. Azzoni, L. Bevilacqua, V. Spandri, S. Kaleci, A. Zoeir, M. C. Sighinolfi, S. Micali, G. Bianchi, G. Pellacani, B. Rocco, R. Montironi, *Virchows Arch.* **2020**, *476*, 511.
- [9] S. Puliatti, L. Bertoni, G. M. Pirola, P. Azzoni, L. Bevilacqua, A. Eissa, A. Elsherbiny, M. C. Sighinolfi, J. Chester, S. Kaleci, B. Rocco, S. Micali, I. Bagni, L. R. Bonetti, A. Maiorana, J. Malvey, C. Longo, R. Montironi, G. Bianchi, G. Pellacani, *BJU Int.* **2019**, *124*, 469.
- [10] R. M. Rezende, M. E. Lopes, G. B. Menezes, H. L. Weiner, *J. Vis. Exp.* **2019**, 150.
- [11] S. Krishnamurthy, A. Cortes, M. Lopez, M. Wallace, S. Sabir, K. Shaw, G. Mills, *Arch. Pathol. Lab Med.* **2018**, *142*, 396.
- [12] I. S. Bagci, R. Aoki, S. Krammer, T. Ruzicka, M. Sardy, L. E. French, D. Hartmann, *J. Eur. Acad. Dermatol. Venereol.* **2019**, *33*, 2123.
- [13] I. S. Bagci, R. Aoki, S. Krammer, T. Ruzicka, M. Sardy, D. Hartmann, *J. Biophotonics* **2019**, *12*, e201800425.
- [14] L. Bertoni, P. Azzoni, C. Reggiani, A. Pisciotto, G. Carnevale, J. Chester, S. Kaleci, L. Reggiani Bonetti, A. M. Cesinaro, C. Longo, G. Pellacani, *Exp. Dermatol.* **2018**, *27*, 1152.
- [15] I. S. Bağcı, R. Aoki, G. Vladimirova, M. Sárdy, T. Ruzicka, L. E. French, D. Hartmann, *J. Biophotonics* **2020**, *13*, e202000328.
- [16] I. S. Bağcı, R. Aoki, G. Vladimirova, E. Ergün, T. Ruzicka, M. Sárdy, L. E. French, D. Hartmann, *Exp. Dermatol.* **2021**, *30*, 684.
- [17] I. S. Bağcı, R. Aoki, S. Krammer, G. Vladimirova, T. Ruzicka, M. Sárdy, L. E. French, D. Hartmann, *J. Biophotonics* **2020**, *13*, e202000328.
- [18] I. S. Bağcı, R. Aoki, S. Krammer, T. Ruzicka, M. Sárdy, D. Hartmann, *J. Biophotonics* **2019**, *12*, e201800425.
- [19] C. Longo, M. Ragazzi, M. Rajadhyaksha, K. Nehal, A. Bennassar, G. Pellacani, J. M. Guiler, *Dermatol. Clin.* **2016**, *34*, 497.
- [20] D. Hartmann, C. Ruini, L. Mathemeier, A. Dietrich, T. Ruzicka, T. von Braunmuhl, *J. Biophotonics* **2016**, *9*, 376.
- [21] D. Hartmann, S. Krammer, M. R. Bachmann, L. Mathemeier, T. Ruzicka, T. von Braunmuhl, *J. Biophotonics* **2018**, *11*, e201800062.
- [22] J. Perez-Anker, S. Ribero, O. Yelamos, A. Garcia-Herrera, L. Alos, B. Alejo, M. Combalia, D. Moreno-Ramirez, J. Malvey, S. Puig, *Br. J. Dermatol.* **2020**, *182*, 468.
- [23] C. Longo, R. Pampena, C. Bombonato, S. Gardini, S. Piana, M. Mirra, M. Raucci, A. Kyrgidis, G. Pellacani, M. Ragazzi, *Br. J. Dermatol.* **2019**, *180*, 1473.
- [24] M. Schuurmann, M. M. Stecher, U. Paasch, J. C. Simon, S. Grunewald, *J. Eur. Acad. Dermatol. Venereol.* **2020**, *34*, 1496.

- [25] C. Longo, M. Rajadhyaksha, M. Ragazzi, K. Nehal, S. Gardini, E. Moscarella, A. Lallas, I. Zalaudek, S. Piana, G. Argenziano, G. Pellacani, *Br. J. Dermatol.* **2014**, *171*, 561.
- [26] A. Bennàssar, A. Vilata, S. Puig, J. Malvehy, *Br. J. Dermatol.* **2014**, *170*, 360.
- [27] J. B. Taxy, *Arch. Pathol. Lab. Med.* **2009**, *133*, 1135.
- [28] S. R. Mercuri, N. Rizzo, F. Bellinzona, R. Pampena, P. Brianti, G. Moffa, L. Colombo Flink, P. Bearzi, C. Longo, G. Paolino, *Dermatol. Ther.* **2019**, *32*, e13127.

How to cite this article: C. Ruini, G. Vladimirova, B. Kendziora, S. Salzer, E. Ergun, E. Sattler, L. E. French, D. Hartmann, J. *Biophotonics* **2021**, *14*(8), e202100094. <https://doi.org/10.1002/jbio.202100094>